Title
Polyserotonin Nanoparticles as Multifunctional Materials for Biomedical Applications

Journal
ACS Nano, 12(5)

ISSN
1936-0851

Authors
Nakatsuka, Nako
Hasani-Sadrabadi, Mohammad Mahdi
Cheung, Kevin M
et al.

Publication Date
2018-05-22

DOI
10.1021/acsnano.8b01470

Peer reviewed

HHS Public Access

Author manuscript

ACS Nano. Author manuscript; available in PMC 2018 August 11.

Published in final edited form as:

ACS Nano. 2018 May 22; 12(5): 4761–4774. doi:10.1021/acsnano.8b01470.

Polyserotonin Nanoparticles as Multifunctional Materials for Biomedical Applications

Nako Nakatsuka[1,2], **Mohammad Mahdi Hasani-Sadrabadi**[1,2,3,4], **Kevin M. Cheung**[1,2], **Thomas D. Young**[1,2], **Ghasem Bahlakeh**[5], **Alireza Moshaverinia**[1,3], **Paul S. Weiss**[1,2,6,*], and **Anne M. Andrews**[1,2,7,*]

[1]California NanoSystems Institute, University of California, Los Angeles, Los Angeles, CA 90095, United States

[2]Department of Chemistry & Biochemistry, University of California, Los Angeles, Los Angeles, CA 90095, United States

[3]Weintraub Center for Reconstructive Biotechnology, Division of Advanced Prosthodontics, School of Dentistry, University of California, Los Angeles, Los Angeles, California 90095, United States

[4]Parker H. Petit Institute for Bioengineering and Bioscience, G.W. Woodruff School of Mechanical Engineering, Georgia Institute of Technology, Atlanta, Georgia 30332, United States

[5]Department of Engineering and Technology, Golestan University, Aliabad Katool, Iran

[6]Department of Materials Science and Engineering, University of California, Los Angeles, Los Angeles, CA 90095, United States

[7]Semel Institute for Neuroscience & Human Behavior and Hatos Center for Neuropharmacology, University of California, Los Angeles, Los Angeles, CA 90095, United States

Abstract

Serotonin-based nanoparticles represent a class of previously unexplored multifunctional nanoplatforms with potential biomedical applications. Serotonin, under basic conditions, self-assembles into monodisperse nanoparticles *via* autoxidation of serotonin monomers. To demonstrate potential applications of polyserotonin nanoparticles for cancer therapeutics, we show that these particles are biocompatible, exhibit photothermal effects when exposed to near-infrared radiation, and load the chemotherapeutic drug doxorubicin releasing it contextually and responsively in specific microenvironments. Quantum mechanical and molecular dynamics

[*]**Corresponding Authors:** aandrews@mednet.ucla.edu, psw@cnsi.ucla.edu.

Author Contributions

N.N. and M.M.H. designed the experiments. N.N., M.M.H., K.M.C., and T.D.Y. conducted the experiments. G.B. designed and performed the calculations and simulations with input from all authors. All authors performed the data analysis and interpreted the results. N.N., M.M.H., G.B., P.S.W., and A.M.A. wrote the manuscript with input from all authors.

ASSOCIATED CONTENT

Supporting Information

The Supporting Information is available free of charge on the ACS Publications website at DOI: XXX

Results of molecular dynamics simulations, atomic force microscopy images, and measurements of particles, toxicity studies, near-infrared heating studies, and drug-loading studies.

The authors declare no competing financial interests.

simulations were performed to interrogate the interactions between surface-adsorbed drug molecules and polyserotonin nanoparticles. To investigate the potential of polyserotonin nanoparticles for *in vivo* targeting, we explored their nano-bio interfaces by conducting protein corona experiments. Polyserotonin nanoparticles had reduced surface-protein interactions under biological conditions compared to polydopamine nanoparticles, a similar polymer material widely investigated for related applications. These findings suggest that serotonin-based nanoparticles have advantages as drug-delivery platforms for synergistic chemo- and photothermal therapy associated with limited nonspecific interactions.

Table of Contents/Abstract Graphic:

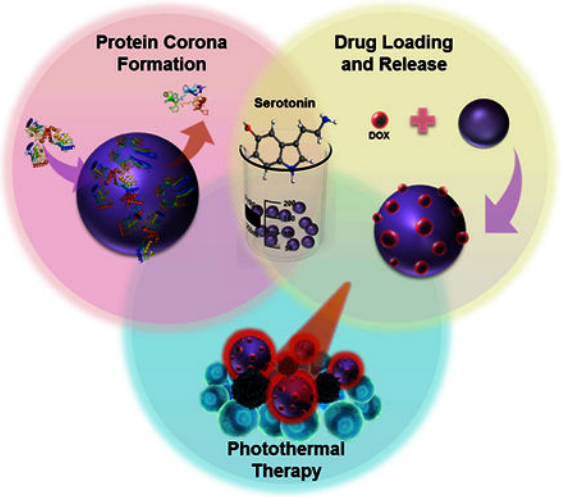

Keywords

serotonin; polydopamine; protein corona; drug delivery; nano-bio interface; mass spectrometry; quantum mechanics; molecular dynamics

Challenges associated with implementing the use of nanoparticles *in vivo* arise from poor understanding and control of surface interactions at the nano-bio interface.[1] Immediately following dispersion in physiological fluids, nanoparticles are coated with proteins to form a protein corona,[2–4] which then determines particle physicochemical properties.[5–8] The corona defines the biological identity of nanoparticles, which directly manifests in interactions with cells and thus, influences critical parameters including cytotoxicity[9,10] and endocytosis into specific cell types.[11–14] Therefore, the protein corona of nanoparticles must be optimized prior to implementation for specific biomedical applications.[15–17]

Polydopamine (PDA) nanoparticles[18] have been proposed for use in a variety of biomedical applications in drug delivery,[19–21] cancer therapeutics,[22–24] antimicrobial applications,[25,26] bone and tissue engineering,[27–30] and cell adhesion and patterning.[31,32] Despite these *in vitro* demonstrations, most have failed to be translated successfully *in vivo*.[33] This challenge may arise from the protein corona surrounding PDA nanoparticles, which has not been thoroughly characterized, and results in nanoparticle-protein interactions with undesired

effects. The highly adhesive properties of PDA may accelerate coating,[34] leading to promiscuous protein coatings that result in delivery and uptake issues depending on specific targets. While drug-delivery capabilities of PDA-based nanoparticles have been shown,[19,20,23,35,36] the structure of PDA and the mechanism of polymerization have not yet been elucidated and thus, surface interactions between adsorbed drug molecules and nanoparticle surfaces remain to be investigated.[37]

Inspired by PDA nanoparticles, we designed and developed nanoparticles based on the autoxidation of serotonin (5-hydroxytryptamine). We discovered that under basic pH conditions, serotonin self-assembles into nanoparticles. In addition to facile synthesis, oxidized serotonin showed reduced adhesive properties compared to PDA. We compared the protein corona that adheres to the surface of polyserotonin *vs*. PDA nanoparticles to investigate how different protein-nanoparticle interactions may lead to potential *in vivo* applications. We explored the potential of polyserotonin nanoparticles as multifunctional nanomaterials for use in cancer therapeutics by testing photothermal properties, drug loading and release, and biocompatibility. To understand molecular interactions at the relevant nano-bio interfaces, we employed quantum mechanics computations and molecular dynamics simulations to model the loading of a chemotherapeutic drug, doxorubicin (DOX). This work suggests that serotonin-based nanoplatforms can serve as versatile scaffolds for combined, synergistic chemo- and photothermal cancer therapeutics, while exhibiting reduced nonspecific adhesion of proteins encountered *in vivo*.

RESULTS AND DISCUSSION

Synthesis and Characterization of Serotonin Nanoparticles.

We incubated serotonin monomers under alkaline conditions (2 mg/mL in phosphate buffer, pH 9.5) to form serotonin nanoparticles (Figure 1a). While this synthesis method did not require a catalyst, the kinetics of polyserotonin nanoparticle formation were substantially slower than dopamine polymerization, which has been reported to be on the order of minutes.[38] Conventionally, polydopamine (PDA) nanoparticles are synthesized by the oxidation and self-polymerization of dopamine in mixtures containing water, ethanol, and ammonia at room temperature.[22] As with PDA formation,[39] the oxidation process of serotonin can be monitored *via* the appearance of a UV absorption peak with time, coupled with a color change of the solution from colorless to dark brown (Figure 1b). Serotonin incubated under mildly acidic conditions (pH 6) did not show additional absorption peaks or a solution color change even after five days.

Polyserotonin nanoparticles were visualized by scanning electron microscopy (SEM) (Figure 1c). The average particle size was ~440 nm after five days of incubation determined by dynamic light scattering (DLS) measurements (Figure 1d). A polydispersity index of 0.06 indicated single size modes with minimal aggregates.[40] We carried out DLS measurements for particles synthesized over 10 days (Figure S1). We found that the size distributions of polyserotonin nanoparticles broaden considerably after seven days with polydispersity indices exceeding 0.5 indicating aggregation.

The zeta potential of serotonin nanoparticles showed a sharp peak at approximately -45 mV, indicative of an overall negative surface charge (Figure 1e). Serotonin monomers have two protonation sites, an aliphatic amino group and an aromatic hydroxyl moiety with pK_a values of 9.97 and 10.73, respectively.[41,42] Since serotonin nanoparticles were synthesized at pH 9.5, which is close to the pK_a of the amino group of serotonin, we expected these particles to be composed of a mixture of cationic (protonated amino group) and neutral (deprotonated amino group) serotonin. Nonetheless, we observed a negative surface charge for the serotonin nanoparticles.

The zeta potential of PDA films has been shown to be -40 mV, similar to polyserotonin nanoparticles.[43] Dopamine has three pK_a values—two phenolic hydroxyl groups with pK_a values of 9.44 and 12.8 and a primary amine with $pK_a = 10.75$.[44] While the precise mechanism of dopamine polymerization remains incompletely determined, it has been hypothesized that polymerization involves the oxidation of dopamine catechol groups to quinones in a pathway reminiscent of melanin formation.[18] The melanin biosynthetic pathway involves hydroxylation of the amino acid tyrosine to 3,4-dihydroxyphenylalanine (*L*-DOPA), which is then oxidized to *o*-dopaquinone followed by polymerization to form melanin.[45] The negative zeta potential for PDA films is predicted to originate from deprotonation of quinone oxygen atoms ($pK_a = 6.3$) at a pH of 8.5. Consequently, we hypothesized that serotonin, an indole neurotransmitter, undergoes similar oxidation, polymerization, and deprotonation to rationalize the resulting negative surface charge.

X-ray photoelectron spectroscopy was performed to identify the composition and chemical bonding of polyserotonin nanoparticles. Serotonin hydrochloride incubated in mildly acidic phosphate buffer (pH 6.5) to inhibit polymerization was used to investigate differences in the chemical bonding characteristics of monomeric serotonin *vs.* oxidized serotonin that forms nanoparticles. The lack of serotonin nanoparticle formation at a mildly acidic pH, even after five days, was confirmed *via* SEM.

The elements present in monomeric serotonin (*i.e.*, carbon, oxygen, and nitrogen), appear in the respective spectra for the base-treated nanoparticles (Figure 2a,b). The C 1s regions for the serotonin monomers and nanoparticles can be fit with four peaks corresponding to C–H/C–NH_2 (285 eV), C–O/C–N (286 eV), C=O/C=N (288 eV), and $\pi \rightarrow \pi^*$ (291 eV) species.[38,46] While the basic peak shapes for both spectra are similar, the peak intensities corresponding to oxygen functional groups are more dominant in the nanoparticle case, suggesting that serotonin was indeed oxidized. The O 1s regions for both samples can be fit with two peaks corresponding to O=C (531 eV) and O–C (533 eV) species.[38,46] It should be noted that the additional peak at 535 eV, seen in Figure 2e, results from overlap with the Na KLL Auger peak.[46] While the N 1s regions for the serotonin monomers and nanoparticles have peaks corresponding to R–NH_2 (402 eV) and R–NH–R (400 eV), there are additional peaks corresponding to =N–R (399 eV) and oxidized nitrogen functionalities (403 eV) for the polyserotonin nanoparticles.[47,48,46–48] Together, these additional peaks indicate that oxidized serotonin likely polymerizes to form nanoparticles.

We investigated polyserotonin nanoparticles using peak-force atomic force microscopy (PF-AFM), an intermittent contact mode used to measure the topography and nanomechanical

properties of materials. The AFM topography map in Figure 2c shows polyserotonin nanoparticles having diameters of approximately 500 nm. Diameters measured by AFM are consistent with those determined *via* SEM and DLS.

We used PF-AFM to measure the adhesion force, the force required to retract an AFM tip from a surface, of the polyserotonin nanoparticles in comparison to PDA nanoparticles. As shown in the adhesion maps and corresponding line sections for polyserotonin (Figure 2c; Figure S2a) *vs.* PDA (Figure S2b,c), differences in adhesion between these nanoparticles and Au substrates was almost four times greater for PDA (~23 nN) compared to polyserotonin (~6 nN). Thus, PDA is significantly more adhesive than polyserotonin. We note that PDA promotes biological adhesion under native conditions in mussels.[18,49]

Protein Corona.

One of the main criteria in selecting nanoparticles for biomedical applications is their level of interaction with proteins in biological environments. Interfacial interactions of nanoparticles with various blood proteins alters therapeutic functionality in an unpredictable manner.[50] In 2007, the term “protein corona” emerged to describe the spontaneous self-assembly and layering of proteins onto nanoparticle surfaces.[2,4] Despite nanoparticle surface functionalization strategies aimed at reducing protein adsorption, there is currently no strategy to eliminate protein corona formation fully.[51] We hypothesized that the reduced adhesive properties of polyserotonin *vs.* PDA nanoparticles would decrease protein corona formation on the surfaces of the former.

To assess differences in adhesive properties between polyserotonin and PDA nanoparticles and to investigate whether surface adhesion influences protein adsorption directly, we analyzed the adsorption of >100 proteins using liquid-chromatography mass-spectrometry (LC-MS) (Figure 3a).[52] Depending on the nature of each protein and the nanoparticle surfaces, some proteins associated weakly and quickly dissociated (soft corona), while others bound strongly and irreversibly (hard corona).[2,53] Polyserotonin nanoparticles adsorbed 35% fewer identified plasma proteins compared to PDA nanoparticles, possibly due to the lower surface adhesion as determined by PF-AFM (Figures 2c and S2).

Fibrinogen, a coagulation protein, was found to be the major plasma protein in the hard corona for polyserotonin- and PDA-based nanoparticles (Figure 3b). High adsorption levels of fibrinogen have been reported for hydrophilic nanoparticle surfaces and amine-modified quantum dots,[54] with adsorption occurring at significantly higher levels than for other adhesion proteins.[55] Fibrinogen surface adhesion is problematic for *in vivo* delivery because it triggers activation of the immune system *via* hemostasis and leukocyte activation.[56,57]

Serum albumin was the protein with the second highest surface adsorption abundance for polyserotonin and PDA nanoparticles. Bovine serum albumin has been used to coat the surfaces of drug delivery carriers to form “stealth” nanoparticles with prolonged blood circulation times.[58] Preformed albumin coronas have also been shown to be a strategic way to decrease nonspecific adsorption of other immune-triggering proteins and to decrease the clearance rates of nanoparticles.[59–61] Thus, having a high surface coverage of serum albumin may, in fact, be advantageous for the nanoparticles investigated here. The

complement system is the first line of defense against foreign materials that cause inflammation and damage to the host.[62,63] Relatively low levels of complement proteins were found on the surfaces of polyserotonin and PDA nanoparticles, which may result in longer blood circulation times for these nanoparticles.[64]

Coating nanoparticles with the hydrophilic polymer, polyethylene glycol (PEG), has been shown to impart steric stabilization and to reduce surface adhesion of blood proteins, thereby prolonging circulation half-lives *in vivo*.[65] To this end, we coated polyserotonin and PDA nanoparticles with PEG *via* incubation of nanoparticles with PEG-SH at basic pH (~8.5) for 24 h. As shown in Figure 3b, PEGylation of polyserotonin and PDA nanoparticles reduced total protein adsorption levels by ~70%. Post-PEGylation, total adsorbed proteins were comparable for polyserotonin and PDA nanoparticles despite differences in adhesion characteristics prior to PEGylation. That the PEGylation of nanoparticles reduces protein corona formation to comparable values for the two types of nanoparticles supports our hypothesis that surface adhesive properties significantly influence protein adsorption. For both nanoparticles, post-PEGylation, fibrinogen adhesion was reduced by ~85%, which suggests that these PEGylated nanoparticles may evoke reduced immunological responses when exposed to *in vivo* environments.

Clusterin, a lipoprotein, was found to be the major protein in the hard corona of PEGylated polyserotonin and PDA nanoparticles. High levels of clusterin adsorption were previously reported for other PEGylated,[66,67] silica-[68] and lipid-based[69] nanoparticles. It has been hypothesized that clusterin adhesion on the surfaces of PEGylated nanoparticles induces a stealth effect and inhibits nanoparticle uptake by phagocytes.[70] Thus, immunotoxicity can be mitigated or augmented depending on the types of nanoparticles and adsorbed plasma proteins.[71] Here, analyzing the protein corona of four different nanoparticle compositions demonstrated the importance of investigating nano-bio interfaces at nanoparticle surfaces, which will enable choices of delivery vehicles depending on the targeting application and experimental design.

Cell Viability.

Human-derived stem cells were incubated with polyserotonin nanoparticles at different concentrations ranging from 1 to 400 μg/mL to assess cytotoxicity. A standard 3-(4,5-dimethylthiazol-2-yl)-2,5-diphenyltetrazolium bromide (MTT) assay was used to quantify cell viability at two different time points. As shown in Figure 4, even after 72 h in culture, >90% cell viability was observed at lower concentrations (1–25 μg/mL) of polyserotonin nanoparticles. At elevated concentrations (>25 μg/mL), reduced viability was observed only after 72 h for gingival-derived mesenchymal stem cells (GMSCs), while decreases in viability for human dental pulp stem cells (DPSCs) or human bone-marrow mesenchymal stem cells, (hBMMSCs) were not statistically significant. Furthermore, after 72 h exposures, polyserotonin nanoparticles were associated with lower cytotoxicity than PDA counterparts (Figure S3). Upon incubation with 100 μg/mL PDA nanoparticles, statistically significant reductions in cell viability ($P<0.01$) were observed in all three stem cell lines.

Photothermal Therapy and *In Vitro* Drug Release.

Mild photothermal heating (~45 °C) has been shown to improve cancer treatment efficacy by enhancing cellular uptake of chemotherapeutics or triggering intracellular drug release from nanocarriers without causing cell necrosis.[72,73] Near-infrared (NIR)-triggered nano-drug carriers have been explored for combination cancer therapy.[74,75] It has been reported that PDA-based nanoparticles can kill cancerous cells and suppress tumor growth *via* photothermal effects induced by NIR irradiation.[22] We investigated whether polyserotonin nanoparticles display similar properties.

Figure 5a shows the change in temperature of Dulbecco's Modified Eagle Medium (DMEM) media over time during laser irradiation of different polyserotonin nanoparticle concentrations. The maximum temperature change for media alone was <5°C. Samples with polyserotonin nanoparticles (>100 μg/mL) showed temperature increases greater than 20 °C after NIR irradiation, as shown in Figure 5b. We observed that at 200 μg/mL nanoparticles, the temperature increase was higher for PDA compared to polyserotonin (P<0.05; Figure S4).

In addition to targeted heat therapy, we explored drug loading (Figure 5c) and delivery capabilities (Figure 5d) of polyserotonin nanoparticles. Doxorubicin (DOX) is an anticancer chemotherapeutic, which is used extensively in the treatment of solid tumors and acute leukemias.[76] Akin to PDA nanoparticles, we hypothesized that polyserotonin nanoparticles could be used for DOX loading by means of surface adsorption *via* π-π stacking and hydrophobic interactions.[24,77,36]

Comparative studies of the loading efficiencies of polyserotonin *vs.* PDA nanoparticles are shown in Figure S5. The PDA nanoparticles showed greater loading efficiencies at various DOX:nanoparticle ratios. This may be due to differences in surface-exposed functional groups available post-polymerization, which alter the extent of interfacial intermolecular interactions between nanoparticle surfaces and DOX. This phenomenon illustrates the importance of interrogating molecular-level interactions at interfaces to improve the design of drug delivery vectors for specific applications.

The *in vitro* drug release profiles of DOX-loaded polyserotonin nanoparticles in PBS (37 °C) at different pH values are shown in Figure 5d. At pH 7.4, polyserotonin nanoparticles exhibited slow DOX release over 100 h. However, at pH 6.5 (mimicking tumor microenvironments) and pH 5.5 (mimicking intracellular endosomal environments), polyserotonin nanoparticles showed significantly faster release profiles compared to release at pH 7.4. Nanoparticle drug release in endosomal compartments is important because nanoparticles enter cells *via* endocytosis into endosomes. Here, drug release prior to lysosomal secretion is advantageous. These results are promising for localized cancer therapy delivery where the loaded drug would not be fully released from the surface of polyserotonin nanoparticles while in circulation, but could be liberated upon reaching acidic tumor microenvironments.

With regard to lysosomal environments, we investigated the stability of polyserotonin nanoparticles (preformed at pH 9.5 for five days) under acidic drug-release conditions (pH

5.5). Polyserotonin nanoparticles immediately began aggregating under acidic conditions with polydispersity indices exceeding 0.5. After 24 h, particle sizes measured by DLS were >2000nm. This aggregation may increase photothermal effects in acidic tumor microenvironments and enhance therapeutic efficacy.[78]

Polyserotonin nanoparticles thus have the potential to be used as combination cancer therapeutic agents *via* photothermal effects, as well as efficient loading and release of the anticancer drug DOX. A critical requirement for an improved cancer therapeutic is the ability to maximize lethal effects at tumor cell sites. We examined the toxicity of unloaded *vs*. DOX-loaded polyserotonin nanoparticles with and without laser irradiation. Similar to cell viability results previously performed with stem-cell lines (Figure 4), polyserotonin nanoparticles alone were not cytotoxic to HeLa cells, even at high concentrations (200 μg/mL). By contrast, DOX-loaded polyserotonin nanoparticles reduced HeLa cell viability significantly in a concentration-dependent manner ($P<0.001$ at concentrations >25μg/mL; $P<0.01$ at 25μg/mL; and $P<0.05$ for 10μg/mL; Figure 5e). Viability of HeLa cells in the presence of DOX-loaded polyserotonin nanoparticles was comparable to DOX alone, indicating that DOX loaded on polyserotonin nanoparticles is released efficiently and retains cytotoxicity.

Laser irradiation of PDA-coated nanoparticles has been shown to ablate tumors *via* localized increases in temperature.[79] Similar to PDA, upon irradiation with NIR energy, the death rates of cancer cells were significantly increased and dependent on polyserotonin nanoparticle concentrations (Figure 5e). Effects were more pronounced at higher polyserotonin nanoparticle concentrations ($P<0.001$ at concentrations >25μg/mL; $P<0.05$ at 25μg/mL; and *ns* for lower concentrations) and were more notable for DOX-loaded polyserotonin nanoparticles, which showed ~80% cytotoxicity at a concentration of 50μg/mL. Figure 5f shows the estimated half maximal inhibitory concentrations (IC_{50}) for polyserotonin-based nanotherapeutics. While polyserotonin nanoparticles alone were nontoxic, the synergistic cytotoxic effect of DOX-loaded nanoparticles post-laser exposure reduced the required doses of this nanotherapeutic by 40% and 100% compared to DOX or laser treatment alone, respectively.

We further investigated the toxicity of DOX and laser irradiation therapy on non-cancerous cells. Compared to HeLa cell viability, we observed that hBMMSC viability is significantly greater, especially at higher concentrations of polyserotonin nanoparticles loaded with DOX (Figure S6; $P<0.001$ at 200μg/mL; $P<0.01$ for 50–100μg/mL; $P<0.05$ for 25 μg/mL; and *ns* for lower concentrations). The increased viability of stem cells suggests that DOX-loaded polyserotonin nanoparticles have reduced toxicity in non-cancerous cells. For the combined DOX and laser irradiation treatment, we observed that at high nanoparticle concentrations (200μg/mL), stem cell lines were ablated to a similar extent as HeLa cells. However, at lower concentrations of polyserotonin nanoparticles, stem cell viability was significantly higher even after combined DOX and laser treatment ($P<0.01$ for 25–100 μg/mL; *ns* for lower concentrations), suggesting that this combination therapy has the potential of targeting cancerous cells with reduced toxicity to surrounding cells.

Modeling Polyserotonin-Doxorubicin Interactions.

To obtain electronic- and atomic-level information on specific interactions between DOX and serotonin-based nanostructures, quantum mechanical (QM) computations and all-atom molecular dynamics (MD) simulations were performed. Figure 6a depicts geometry-optimized DOX-serotonin clusters extracted from density functional theory (DFT) computations at the M06–2X/6–311G(d,p) levels. From these lowest energy geometries, it is evident that different DOX functional groups, including hydroxyl (-OH), carbonyl (-C=O), and amino ($-NH_2$) groups, are involved in intermolecular hydrogen-bonding interactions with the hydroxyl and primary amino groups of serotonin. This theoretical outcome suggests a central role for hydrogen-bonding in DOX adhesion to serotonin nanoparticle surfaces. Furthermore, in one of the hybrid clusters, the aromatic backbone of serotonin is aligned with a parallel orientation relative to the aromatic heterocycles of DOX, indicating the possibility of **π-π** interactions between DOX and serotonin.

The DOX-serotonin binding affinity ($\Delta E_{binding}$) was calculated as follows: $\Delta E_{binding} = E_{cluster} - (E_{DOX} + E_{serotonin})$. In this expression, $E_{cluster}$ is the potential energy of the optimized DOX-serotonin clusters, and E_{DOX} and $E_{serotonin}$ represent the potential energies of the isolated DOX and serotonin molecules, respectively. The computed $\Delta E_{binding}$ for all hybrid clusters determined from two different levels of M06–2X/6–311G(d,p) and B3LYP/6–311(d,p) calculations are presented in Figure 6a. All $\Delta E_{binding}$ energies were negative, which quantitatively validates DOX-serotonin interactions. Note that the higher binding energy values derived from DFT calculations with the M06–2X exchange-correlation functional compared to those with B3LYP are due to the ability of the former to capture the contributions of weakly bonded complexes and noncovalent interactions.[80,81]

Atomistic MD simulations were performed to investigate *dynamic* interactions between DOX and serotonin clusters. Prior to analysis, the equilibria of the simulation cells were verified by monitoring the thermodynamic potential energies and temperature parameters (Figure S7). Both the potential energy and temperature of all simulated cells stabilized with negligible fluctuations, indicating that equilibria had been reached.[82–84] The final structures of DOX on the surfaces of serotonin and its dimers and tetramers are shown in Figure 6b, which were obtained from the last step of the MD simulations. When these snapshots were compared with the corresponding initial cells (Figure S8), we found that DOX distances relative to all serotonin substrates were significantly reduced, which suggests the tendency of DOX molecules to adsorb on all investigated surfaces. When the MD simulations were continued for longer times, the relative positions of surface-bound DOX did not change, indicating stabilized interfacial adhesion.

Similar to the QM calculations, binding energies for this system were quantified as follows: $\Delta E_{binding} = E_{surface/DOX} - (E_{surface} + E_{DOX})$ (Figure 6b).[85,83,86] Here, $E_{surface/DOX}$, $E_{surface}$, and E_{DOX} are, respectively, the potential energies of an entire cell (*i.e.*, DOX adsorbed on a serotonin surface), an isolated serotonin-based surface, and an isolated DOX molecule. The $\Delta E_{binding}$ values were calculated to be negative in all cases, indicating adhesion between DOX and the serotonin structures, with the strongest adhesion occurring between DOX and the serotonin monomer (-90kcal/mol). Strong monomer binding to DOX suggests the importance of the accessibility of the hydroxyl and amine moieties of serotonin, as well as

conformational freedom for formation of hydrogen bonds. Nonetheless, DOX adsorbed to all modeled structures, including serotonin dimers and tetramers, which supports the experimental findings that DOX is loaded onto polyserotonin nanoparticle surfaces (Figure 5c). Further examination of DOX interfacial interactions *via* simulation snapshots (Figure 6b) suggests that, in agreement with the QM results, hydrogen-bonding interactions play key roles in the adsorption of DOX onto serotonin and polyserotonin surfaces.

Radial distribution functions (RDFs, also called paired correlation functions, g(r)) were analyzed[84] to elucidate DOX interactions with polyserotonin nanoparticle surfaces further. The RDF analysis was carried out for the oxygen atoms in DOX with regard to oxygen and nitrogen heteroatoms in serotonin monomers, dimers, and tetramers (Figure 6c,d). As shown in Figure 6c, the RDFs for DOX oxygen atoms with respect to serotonin monomer, dimer, and tetramer oxygen atoms showed heightened first peaks, particularly for serotonin and dimer-1 at 2.62–2.97Å. These peak positions are within the distances required for hydrogen-bonding interactions[84] between oxygenated sites in DOX and serotonin species.

For serotonin monomers, the alignment of oxygen atoms at optimal hydrogen bonding distances from DOX is likely due to the smaller size and spatial freedom of a single serotonin molecule. For dimer-1 (Scheme 1), the coupling *via* the amine of one monomer to the hydroxyl of the second monomer renders the sterically hindered indole groups at a maximum distance apart. In contrast, the coupling scheme for dimer-2 results in the indole groups side-by-side and separated by a single carbon-carbon bond, which may lead to difficulties in aligning the molecules in close proximity to DOX in the correct orientation for hydrogen bonding. For dimer-2, increased **π**-**π** stacking of aromatic moieties may compensate for reduced hydrogen bonding, which may result in comparable binding energies (-70 kcal/mol) seen in MD simulations (Figure 6b).

Similarly, the DOX oxygen-atom RDFs relative to the nitrogen atoms of serotonin, and its dimers and tetramers possessed high peaks that were of lower intensities at larger distances. These findings suggest that the oxygenated DOX fragments are also involved in interfacial hydrogen bonds with the nitrogenous groups of serotonin-based species. These RDF results are in agreement with the geometry-optimized DOX-serotonin clusters derived from QM computations. Visualized MD snapshots further suggest DOX loading on serotonin nanoparticle surfaces largely through hydrogen-bonding interactions.

Together, the theoretical computations underscore hydrogen-bonding as a primary mechanism of DOX-polyserotonin nanoparticle loading and rationalize differences in the rates of DOX release from the polyserotonin nanoparticles at lower pH values. Lower pH results in protonation of amine groups on DOX preventing nitrogen hydrogen bonding with hydroxyl groups and disrupting intermolecular forces that anchor DOX to polyserotonin nanoparticles, causing faster drug release. Further, protonation leads to increased hydrophilicity and solubility of DOX in aqueous solutions, which may also contribute to faster release, which could be advantageous for targeted delivery of DOX to acidic environments.[87] Investigating molecular interactions between available surface functional groups of polyserotonin nanoparticles and drug molecules will help to determine which drugs can be loaded onto nanoparticle surfaces for targeted drug-delivery applications.

CONCLUSIONS AND PROSPECTS

We report the synthesis, characterization, and multifunctional application of serotonin-based nanoparticles, a previously unexplored nanomaterial. While polyserotonin nanoparticles showed somewhat decreased photothermal and drug loading capabilities compared to polydopamine nanoparticles, a widely investigated vehicle for cancer therapeutics, polyserotonin nanoparticles showed significantly reduced surface adhesion properties. The latter may be associated with the reduction in protein adsorption on polyserotonin compared to polydopamine nanoparticles. Coating polyserotonin nanoparticles with polyethylene glycol further reduced total protein adsorption when compared to uncoated nanoparticles and notably, decreased the adhesion of fibrinogen, an immune triggering protein by 85%.

Compared to polydopamine, polyserotonin nanoparticles showed improved biocompatibility with stem-cell lines, even at high concentrations (>100 μg/mL) over longer time periods (72 h). Polyserotonin nanoparticles loaded with the cancer therapeutic doxorubicin and irradiated with near-infrared energy showed photothermal/chemotherapeutic effects that decreased cell viability by almost 100%. Polyserotonin nanoparticles are promising chemotherapeutic candidates due to their inherent biocompatibility in the presence of healthy cells coupled to the capacity to be activated in specific environments to kill cancerous cells. Laser irradiation enables controlled cell death at precise times and locations. Polyserotonin nanoparticles also released the anti-cancer drug doxorubicin in a pH-dependent manner to targer tumor microenvironments and enabling synergistic killing of cancer cells.

We conducted quantum mechanical computations and molecular dynamics simulations to investigate interfaces between polymerized serotonin structures and the chemotherapeutic doxorubicin. Our results suggest that hydrogen-bonding plays a critical role in the adsorption of doxorubicin onto serotonin surfaces. These results will guide future studies on the loading efficiencies of different classes of drugs based on intermolecular interactions at interfaces with nanoparticle surfaces. The investigation of molecular interactions of polyserotonin surfaces with drug molecules and serum proteins, in addition to characterizations of cancer therapeutic properties, together demonstrate that polyserotonin nanoparticles are a nanomaterial with potential for future clinical applications.

MATERIALS AND METHODS

Materials.

Gold films (100 nm) overlaying titanium (10 nm) on Si substrates (Au/Si) were purchased from Platypus Technologies (Madison, WI). Serotonin hydrochloride, dopamine (3,4-dihydroxyphenylalanine) hydrochloride, doxorubicin hydrochloride, Tris-HCl, and KH_2PO_4 and K_2HPO_4 (phosphate buffer components) were purchased from Sigma-Aldrich (St. Louis, MO). Dulbecco's Modified Eagle Medium (DMEM) and Pierce bicinchoninic acid (BCA) Protein Assay Kits were purchased from Thermo Fisher Scientific Inc. (Canoga Park, CA). The mPEG-SH, MW 5kDa, was from Creative PEGWorks (Durham County, NC). Deionized water (~18 MΩ) was obtained from a Millipore water purifier (Billerica, MA).

Young (18–25-year-old) healthy male subjects undergoing third molar extractions were selected for extraction of gingival and dental pulp tissues. All procedures involving human subjects were pre-approved by the UCLA Institutional Review Boards, Human Research Protection Program (IRB #BUA6510). Gingival mesenchymal stem cells and dental pulp stem cells were isolated and cultured according to published protocols.[88,89] Human bone marrow mesenchymal stem cells were purchased from Lonza Inc. (Walkersville, MD). Flow cytometry (BD Biosciences, San Jose, CA) was used to determine the stem-cell surface markers STRO-1 and CD146. Cells from passage four were used in all experiments.

Nanoparticle Synthesis.

Serotonin hydrochloride (2 mg/mL) was incubated in phosphate buffer (0.70 mM KH_2PO_4, 500 mM K_2HPO_4, pH 9.5) for 1–10 days to produce polyserotonin nanoparticles. For most experiments, polyserotonin nanoparticles were grown for five days. Polydopamine nanoparticles were synthesized *via* an oxidation and self-polymerization dispersion procedure.[20,24,36] Briefly, dopamine hydrochloride was dissolved in Tris-HCl (10 mM, pH 8.5) and the mixture was stirred in the dark for 16 h to polymerize dopamine at room temperature.

Characterization.

Absorbance measurements were performed using an Evolution 600 spectrophotometer (Thermo Fisher Scientific Inc.). Dynamic light scattering and zeta potential measurements were performed at pH 7.4 using a Zetasizer 3000HS (Malvern Instruments Ltd., Worcestershire, UK). Measurements were conducted in backscattering mode at an angle of 173° for dilute polyserotonin nanoparticle suspensions in water at 37 °C.

Polyserotonin nanoparticles were centrifuged and washed three times in deionized water, drop-cast onto Au/Si substrates, and incubated overnight. Substrates were rinsed with deionized water and blown dry with nitrogen gas prior to imaging with a JSM-6700F field-emission scanning electron microscope (JEOL USA Inc., Huntington Beach, CA) using a 3-kV accelerating potential.

Particles were also imaged by atomic force microscopy using a Dimension Icon scanning probe microscope (Bruker, Billerica, MA). Nanoparticle topographies and mechanical properties simultaneously measured using the PeakForce Quantitative Nanomechanical Property Mapping (PeakForce QNM) mode. ScanAsyst-Air cantilevers (Bruker, spring constant = 0.4 ± 0.1 N/m) were used for all measurements. The peak-force set-point was chosen and adjusted automatically through the ScanAsyst® imaging mode.

An AXIS Ultra DLD X-ray photoelectron spectrometer (Kratos Analytical Inc., Chestnut Ridge, NY) was used for elemental surface analysis. This spectrometer uses a monochromatic Al Kr X-ray source with a 200-μm circular spot size and ultrahigh vacuum (10^{-9} Torr). Spectra were acquired at a pass energy of 160 eV for survey spectra and 20 eV for high-resolution spectra of C 1s, O 1s, and N 1s, regions using a 300-ms dwell time. For both scan types, 15 kV was applied with an emission of 10 mA. Three scans were performed for survey spectra and 10 scans for each of the high-resolution spectra.

Protein Corona Characterization.

Protein corona experiments were performed as reported previously.[90,67] Briefly, venous blood was obtained from ten healthy donors *via* the UCLA/CFA Virology Core Laboratory. Plasma was separated, and protein aggregates were removed by ultracentrifugation. Nanoparticles were incubated with human plasma under gentle shaking for 3 h, separated using ultracentrifugation at 20,000 g for 1 h, and then washed three times. Proteins were then eluted after dissolving nanoparticles by reducing the pH to 3.0 and shaking the solution for 30 min. Protein concentrations were assessed *via* micro-BCA protein assays.

Afterwards, proteins were digested following reported protocols.[68] Quantitative analyses of protein samples were performed by LC-MS. A LTQ Orbitrap XL Mass Spectrometer (Thermo Fisher Scientific Inc.) coupled with an Eksigent NanoLC-2D high-performance liquid chromatograph and autosampler were used after 10-fold dilution of digested protein samples in 0.1% formic acid. The experimental details were as reported by Schöttler *et al.*[67] Mass spectra were collected over a m/z range of 300–2000 Da. All samples were analyzed in triplicate to quantify the amounts of each protein adsorbed on nanoparticle surfaces.

Cell Viability.

Standard MTT colorimetric assays were conducted using hBMMSCs, GMSCs, DPSCs, and a cervical cancer cell line, HeLa cells, to examine nanoparticle-induced cytotoxicity. To determine cell viability, cells were plated at densities of 10,000 cells per well in 96-well plates and incubated overnight at 37 °C in an incubator maintained at 5% CO_2. Cells were then incubated with nanoparticles over a concentration range of 1–400 μg/mL. The culture medium was discarded after 24 or 72 h and cells were washed with PBS (pH 7.4) followed by incubation for 2 h with 100 μL of MTT solution in DMEM (500 μg/mL in phosphate buffer pH 7.4). The medium containing MTT was replaced with 150 μL of dimethyl sulphoxide in each well.

After shaking the plates for 10 min, the absorbance values of the wells were recorded with a microplate reader (Bio-Tek Synergy HT, Winooski, VT) at a wavelength of 570 nm. The control culture medium contained no nanoparticles. All measurements were performed at room temperature. The spectrophotometer was calibrated to zero absorbance using control culture medium containing no cells. The relative cell viability (%) related to the control wells was calculated as:

$$([A]_{test}/[A]_{control}) \times 100$$

where $[A]_{test}$ is the absorbance of the test sample and $[A]_{control}$ is the absorbance of the control sample.

In Vitro Drug Release.

To determine *in vitro* drug release profiles, lyophilized DOX-loaded polyserotonin nanoparticles (1 mg) were dispersed in 1 mL of PBS (pH 7.4). To investigate the loading efficiencies of DOX on the surfaces of polyserotonin nanoparticles, different w/w

concentrations of DOX were added to 1 mg/mL of nanoparticles. The solutions were placed in a 3500 Da MWCO dialysis cartridge (Thermo Scientific, Waltham, MA). Cartridges were then immersed in 1 L of PBS and gently shaken at 37 °C in a water bath. At predetermined intervals, buffered solutions were collected and replaced with equivalent volumes of fresh PBS. The DOX concentrations were measured by spectrophotometry at 430 nm.

Concentrations were evaluated over a linear concentration range. In this range, percent deviations from theoretical values were found to be less than 5% and coefficients of linearity were greater than 0.96 using DOX standards. The DOX concentrations were corrected for sampling effects according to the following equation:

$$C_n^1 = C_n[V_T/(V_T - V_S)](C_{n-1}{}^1/C_{n-1})$$

where C_n^1 is the corrected concentration of the n^{th} sample, C_n is the measured concentration of DOX in the n^{th} sample, C_{n-1} is the measured concentration of the $(n\text{-}1)^{th}$ sample, V_T is the volume of receiver fluid, V_S represents the volume of the sample drawn (1 mL), and C_{n-1}^1 is the corrected concentration of the $(n\text{-}1)^{th}$ sample. Loading efficiencies of the nanoparticles were determined by applying the following equation:

DOX Loading efficiency = (DOX adsorbed to nanoparticles/initial amount of DOX) x 100%.

Photothermal Therapy.

A thermal imaging camera (FLIR Systems; Nashua, NH) was used to record near-infrared laser irradiation-induced increases in temperature (808 nm; 1.5 $W{\cdot}cm^{-2}$). For photothermal ablation of cancer cells, HeLa cells were seeded in tissue culture dishes at a density of 40,000 cells/cm^2 and were cultured for 24 h at 37 °C in an incubator maintained at 5% CO_2 until 80% cell confluence. Next, the medium was replaced with nanoparticle-containing medium (25–400 mg/ml). After incubation for 4 h, the cells were rinsed three times with PBS to remove free nanoparticles. Fresh medium was added and laser light at 808 nm, 1.5 $W{\cdot}cm^{-2}$ with a 250-nm diameter spot-size was irradiated for 6 min. Cell viability was characterized using the MTT assay described above.

Statistics.

One-way analysis of variance followed by Tukey's multiple group comparisons was used to compare the half maximal inhibitory concentrations for polyserotonin-based nanotherapeutics. Two-tailed unpaired Student's *t*-tests were used to compare cell viabilities in the absence of polymeric nanoparticles *vs.* in the presence of maximum concentrations of nanoparticles. Statistics were computed using GraphPad Prism (GraphPad Software Inc., San Diego). All data are reported as means ± standard errors of the means with probabilities $P<0.05$ considered statistically significant.

Quantum Mechanics Computations.

To explore DOX affinity for polyserotonin nanoparticles, *ab initio* quantum mechanical computations employing density functional theorymethods were applied. The molecular

structures of DOX and serotonin are displayed in Scheme 1. As illustrated, a number of oxygenated and nitrogenous moieties are present in DOX and serotonin. Accordingly, to examine interactions between the functional groups of DOX and serotonin, five different starting DOX-serotonin clusters were constructed. These hybrid clusters were subjected to geometry optimizations based on DFT calculations. Within DFT computations, electronic exchange-correlation interactions were taken into account using two different levels of M06–2X[91] and B3LYP calculations, in conjunction with the 6–311G(d,p) basis function.[92–94] Lowest energy geometries were utilized to determine the partial atomic charges of DOX and serotonin, and their binding energies. The electrostatic potential (ESP) -based method, ChelpG, was adopted to analyze the partial charges of geometry-optimized DOX and serotonin for subsequent use in classical atomistic molecular dynamics simulations.[95] All QM computations were carried out using the Gaussian 09 suite of programs.[96]

Construction of Serotonin Surfaces.

Besides first-principles QM computations, classical MD simulations were applied to examine DOX-polyserotonin affinities at larger scales. As the structure of polyserotonin is not known, in addition to serotonin, two different dimers (designated dimer-1 and dimer-2) and two different tetramers (tetramer-1 and tetramer-2), based on the serotonin structure were built to represent polyserotonin. The minimum energy structures of these dimers and tetramers resulting from DFT/B3LYP/6–311G(d,p) are shown in Scheme 1.

To construct surfaces of serotonin, serotonin dimers, and serotonin tetramers, their corresponding energy-minimized structures derived from QM calculations were utilized. First, a serotonin cell consisting of 100 serotonin molecules, two serotonin dimer cells each containing 50 dimers, and two amorphous cells for serotonin tetramers including 25 serotonin tetramers were generated at a lower density of 0.5 g/cm^3 using Materials Studio software.[97] This lower initial density was used for cell construction to equilibrate the generated cells more efficiently. The energies of these five simulation cells were minimized using the Smart minimizer algorithm for 2000 steps and then subjected to NPT MD simulations performed for 250 ps at 1 atm and 300 K. Afterwards, a vacuum space of approximately 30 Å was placed above all equilibrated cells in a direction normal to the surface (defined as the *z*-axis).

Molecular Dynamics Simulations.

To conduct MD simulations, the DFT-optimized DOX geometry was first placed over all five simulation cells at larger distances from each surface. The cells containing serotonin-based adsorbent and DOX adsorbate are depicted in Supplementary Figure S8. Before MD simulations, the potential energies of these cells were minimized by applying the Smart minimizer algorithm for 2000 steps using an accuracy level of “medium”, in which convergence criteria were 0.001 kcal/mol for energy, 0.5 kcal/mol-Å for force, and 0.015 Å for displacement. Subsequently, MD simulations were executed on optimized cells in the NVT ensemble, where N is the number of particles in the system, V is the system volume, and T is the absolute temperature, for 300 ps at room temperature. Periodic boundary conditions (PBCs) were used in all three dimensions of the simulation cells. Both

optimization and dynamics simulations were carried out using the Forcite module, as available in Materials Studio software.[97]

The potential energy parameters required for the calculations of bonded and non-bonded interactions of DOX and serotonin (*i.e.*, monomer, dimers, and tetramers) were taken from the condensed-phase optimized molecular potentials for atomistic simulation studies (COMPASS) force field.[98,99] The *ab initio* force field in COMPASS provides accurate predictions of gas-phase and condensed-phase properties of a range of molecules. This force field has been applied in previous theoretical investigations of organic and inorganic systems.[100,86,99] To describe the electrostatic interactions between serotonin and DOX, their partial atomic charges were adopted from QM computations based on the ChelpG scheme and subsequently used in MD simulations. During MD simulations, both van der Waals and electrostatic interactions were modeled by the Ewald summation scheme. The velocity Verlet method with a time step of 1 fs was applied for the integration of Newton's equation of motion.[101] To control the operational temperature at the desired value of 298 K, the Andersen thermostat was applied. Note that during both static and dynamics steps (*i.e.*, optimization and MD simulation), no constraints were applied to the positions of DOX- and serotonin-based surface atoms.

Supplementary Material

Refer to Web version on PubMed Central for supplementary material.

ACKNOWLEDGMENTS

This research was supported by the Cal-Brain Neurotechnology Program, the National Institute on Drug Abuse (DA045550), the National Institute of Dental and Craniofacial Research (DE023825), and the National Institute of Allergy and Infectious Disease (UCLA/CFAR Virology Core Lab AI028697). The authors would like to thank John M. Abendroth, Profs. Anastassia Alexandrova and Philippe Sautet, and Dr. Kaining Duanmu for helpful discussions.

REFERENCES

(1). Ritz S ; Schottler S ; Kotman N ; Baier G ; Musyanovych A ; Kuharev J ; Landfester K ; Schild H ; Jahn O ; Tenzer S ; Mailander V Protein Corona of Nanoparticles: Distinct Proteins Regulate the Cellular Uptake. Biomacromolecules 2015, 16, 1311–1321.25794196

(2). Cedervall T ; Lynch I ; Lindman S ; Berggard T ; Thulin E ; Nilsson H ; Dawson KA ; Linse S Understanding the Nanoparticle-Protein Corona Using Methods to Quantify Exchange Rates and Affinities of Proteins for Nanoparticles. Proc. Natl. Acad. Sci. U.S.A 2007, 104, 2050–2055.17267609

(3). Walczyk D ; Bombelli FB ; Monopoli MP ; Lynch I ; Dawson KA What the Cell "Sees" in Bionanoscience. J. Am. Chem. Soc 2010, 132, 5761–5768.20356039

(4). Ke PC ; Lin S ; Parak WJ ; Davis TP ; Caruso F A Decade of the Protein Corona. ACS Nano 2017, 11, 11773–11776.29206030

(5). Rocker C ; Potzl M ; Zhang F ; Parak WJ ; Nienhaus GU A Quantitative Fluorescence Study of Protein Monolayer Formation on Colloidal Nanoparticles. Nat. Nanotechnol 2009, 4, 577–580.19734930

(6). Lundqvist M ; Stigler J ; Cedervall T ; Berggard T ; Flanagan MB ; Lynch I ; Elia G ; Dawson K The Evolution of the Protein Corona around Nanoparticles: A Test Study. ACS Nano 2011, 5, 7503–7509.21861491

(7). Tenzer S ; Docter D ; Kuharev J ; Musyanovych A ; Fetz V ; Hecht R ; Schlenk F ; Fischer D ; Kiouptsi K ; Reinhardt C ; Landfester K ; Schild H ; Maskos M ; Knauer SK ; Stauber RH Rapid Formation of Plasma Protein Corona Critically Affects Nanoparticle Pathophysiology. Nat. Nanotechnol 2013, 8, 772–781.24056901

(8). Pelaz B ; Alexiou C ; Alvarez-Puebla RA ; Alves F ; Andrews AM ; Ashraf S ; Balogh LP ; Ballerini L ; Bestetti A ; Brendel C ; Bosi S ; Carril M ; Chan WC ; Chen C ; Chen X ; Chen X ; Cheng Z ; Cui D ; Du J ; Dullin C et al. Diverse Applications of Nanomedicine. ACS Nano 2017, 11, 2313–2381.28290206

(9). Kim JA ; Salvati A ; Aberg C ; Dawson KA Suppression of Nanoparticle Cytotoxicity Approaching *in Vivo* Serum Concentrations: Limitations of *in Vitro* Testing for Nanosafety. Nanoscale 2014, 6, 14180–14184.25340311

(10). Saha K ; Moyano DF ; Rotello VM Protein Coronas Suppress the Hemolytic Activity of Hydrophilic and Hydrophobic Nanoparticles. Mater. Horizons 2014, 1, 102–105.

(11). Hellstrand E ; Lynch I ; Andersson A ; Drakenberg T ; Dahlback B ; Dawson KA ; Linse S ; Cedervall T Complete High-Density Lipoproteins in Nanoparticle Corona. FEBS J 2009, 276, 3372–3381.19438706

(12). Walkey CD ; Chan WCW Understanding and Controlling the Interaction of Nanomaterials with Proteins in a Physiological Environment. Chem. Soc. Rev 2012, 41, 2780–2799.22086677

(13). Fleischer CC ; Payne CK Nanoparticle-Cell Interactions: Molecular Structure of the Protein Corona and Cellular Outcomes. Acc. Chem. Res 2014, 47, 2651–2659.25014679

(14). Fleischer CC ; Payne CK Secondary Structure of Corona Proteins Determines the Cell Surface Receptors Used by Nanoparticles. J. Phys. Chem. B 2014, 118, 14017–14026.24779411

(15). Kah JCY ; Chen J ; Zubieta A ; Hamad-Schifferli K Exploiting the Protein Corona around Gold Nanorods for Loading and Triggered Release. ACS Nano 2012, 6, 6730–6740.22804333

(16). Cifuentes-Rius A ; de Puig H ; Kah JCY ; Borros S ; Hamad-Schifferli K Optimizing the Properties of the Protein Corona Surrounding Nanoparticles for Tuning Payload Release. ACS Nano 2013, 7, 10066–10074.24128271

(17). Walkey CD ; Olsen JB ; Song FY ; Liu R ; Guo HB ; Olsen DWH ; Cohen Y ; Emili A ; Chan WCW Protein Corona Fingerprinting Predicts the Cellular Interaction of Gold and Silver Nanoparticles. ACS Nano 2014, 8, 2439–2455.24517450

(18). Lee H ; Dellatore SM ; Miller WM ; Messersmith PB Mussel-Inspired Surface Chemistry for Multifunctional Coatings. Science 2007, 318, 426–430.17947576

(19). Ho CC ; Ding SJ The pH-Controlled Nanoparticles Size of Polydopamine for Anti-Cancer Drug Delivery. J. Mater. Sci 2013, 24, 2381–2390.

(20). Liu R ; Guo YL ; Odusote G ; Qu FL ; Priestley RD Core-Shell Fe_3O_4 Polydopamine Nanoparticles Serve Multipurpose as Drug Carrier, Catalyst Support and Carbon Adsorbent. ACS Appl. Mater. Inter 2013, 5, 9167–9171.

(21). Zhong XY ; Yang K ; Dong ZL ; Yi X ; Wang Y ; Ge CC ; Zhao YL ; Liu Z Polydopamine as a Biocompatible Multifunctional Nanocarrier for Combined Radioisotope Therapy and Chemotherapy of Cancer. Adv. Funct. Mater 2015, 25, 7327–7336.

(22). Liu YL ; Ai KL ; Liu JH ; Deng M ; He YY ; Lu LH Dopamine-Melanin Colloidal Nanospheres: An Efficient Near-Infrared Photothermal Therapeutic Agent for *in Vivo* Cancer Therapy. Adv. Mater 2013, 25, 1353–1359.23280690

(23). Sasikala ARK ; GhavamiNejad A ; Unnithan AR ; Thomas RG ; Moon M ; Jeong YY ; Park CH ; Kim CS A Smart Magnetic Nanoplatform for Synergistic Anticancer Therapy: Manoeuvring Mussel-Inspired Functional Magnetic Nanoparticles for pH Responsive Anticancer Drug Delivery and Hyperthermia. Nanoscale 2015, 7, 18119–18128.26471016

(24). Dong ZL ; Gong H ; Gao M ; Zhu WW ; Sun XQ ; Feng LZ ; Fu TT ; Li YG ; Liu Z Polydopamine Nanoparticles as a Versatile Molecular Loading Platform to Enable Imaging-Guided Cancer Combination Therapy. Theranostics 2016, 6, 1031–1042.27217836

(25). Cong Y ; Xia T ; Zou M ; Li ZN ; Peng B ; Guo DZ ; Deng ZW Mussel-Inspired Polydopamine Coating as a Versatile Platform for Synthesizing Polystyrene/Ag Nanocomposite Particles with Enhanced Antibacterial Activities. J. Mater. Chem. B 2014, 2, 3450–3461.

(26). Lu ZS ; Xiao J ; Wang Y ; Meng M *In Situ* Synthesis of Silver Nanoparticles Uniformly Distributed on Polydopamine-Coated Silk Fibers for Antibacterial Application. J. Colloid Interf. Sci 2015, 452, 8–14.

(27). Ko E ; Yang K ; Shin J ; Cho SW Polydopamine-Assisted Osteoinductive Peptide Immobilization of Polymer Scaffolds for Enhanced Bone Regeneration by Human Adipose-Derived Stem Cells. Biomacromolecules 2013, 14, 3202–3213.23941596

(28). Luo RF ; Tang LL ; Zhong S ; Yang ZL ; Wang J ; Weng YJ ; Tu QF ; Jiang CX ; Huang N *In Vitro* Investigation of Enhanced Hemocompatibility and Endothelial Cell Proliferation Associated with Quinone-Rich Polydopamine Coating. ACS Appl. Mater. Inter 2013, 5, 1704–1714.

(29). Liu Y ; Ai K ; Lu L Polydopamine and Its Derivative Materials: Synthesis and Promising Applications in Energy, Environmental, and Biomedical Fields. Chem. Rev 2014, 114, 5057–5115.24517847

(30). Gao X ; Song JL ; Ji P ; Zhang XH ; Li XM ; Xu X ; Wang MK ; Zhang SQ ; Deng Y ; Deng F ; Wei SC Polydopamine-Templated Hydroxyapatite Reinforced Polycaprolactone Composite Nanofibers with Enhanced Cytocompatibility and Osteogenesis for Bone Tissue Engineering. ACS Appl. Mater. Inter 2016, 8, 3499–3515.

(31). Chien HW ; Tsai WB Fabrication of Tunable Micropatterned Substrates for Cell Patterning *via* Microcontact Printing of Polydopamine with Poly(Ethylene Imine)-Grafted Copolymers. Acta Biomater 2012, 8, 3678–3686.22765962

(32). Sun K ; Xie YY ; Ye DK ; Zhao YY ; Cui Y ; Long F ; Zhang W ; Jiang XY Mussel-Inspired Anchoring for Patterning Cells Using Polydopamine. Langmuir 2012, 28, 2131–2136.22085048

(33). Caracciolo G ; Farokhzad OC ; Mahmoudi M Biological Identity of Nanoparticles *in Vivo*: Clinical Implications of the Protein Corona. Trends Biotechnol 2017, 35, 257–264.27663778

(34). Lynge ME ; van der Westen R ; Postma A ; Stadler B Polydopamine − A Nature-Inspired Polymer Coating for Biomedical Science. Nanoscale 2011, 3, 4916–4928.22024699

(35). Wang XY ; Zhang JS ; Wang YT ; Wang CP ; Xiao JR ; Zhang Q ; Cheng YY Multi-Responsive Photothermal-Chemotherapy with Drug-Loaded Melanin-Like Nanoparticles for Synergetic Tumor Ablation. Biomaterials 2016, 81, 114–124.26731575

(36). Li WQ ; Wang ZG ; Hao SJ ; He HZ ; Wan Y ; Zhu CD ; Sun LP ; Cheng G ; Zheng SY Mitochondria-Targeting Polydopamine Nanoparticles to Deliver Doxorubicin for Overcoming Drug Resistance. ACS Appl. Mater. Inter 2017, 9, 16794–16803.

(37). Liebscher J ; Mrowczynski R ; Scheidt HA ; Filip C ; Hadade ND ; Turcu R ; Bende A ; Beck S Structure of Polydopamine: A Never-Ending Story? Langmuir 2013, 29, 10539–10548.23875692

(38). Zangmeister RA ; Morris TA ; Tarlov MJ Characterization of Polydopamine Thin Films Deposited at Short Times by Autoxidation of Dopamine. Langmuir 2013, 29, 8619–8628.23750451

(39). Mazario E ; Sanchez-Marcos J ; Menendez N ; Herrasti P ; Garcia-Hernandez M ; Munoz-Bonilla A One-Pot Electrochemical Synthesis of Polydopamine Coated Magnetite Nanoparticles. RSC Adv 2014, 4, 48353–48361.

(40). Nobbmann U ; Morfesis A Light Scattering and Nanoparticles. Mater. Today 2009, 12, 52–54.

(41). Rudnick G ; Kirk KL ; Fishkes H ; Schuldiner S Zwitterionic and Anionic Forms of a Serotonin Analog as Transport Substrates. J. Biol. Chem 1989, 264, 14865–14868.2549040

(42). Pratuangdejkul J ; Nosoongnoen W ; Guerin GA ; Loric S ; Conti M ; Launay JM ; Manivet P Conformational Dependence of Serotonin Theoretical pK_a Prediction. Chem. Phys. Lett 2006, 420, 538–544.

(43). Bernsmann F ; Frisch B ; Ringwald C ; Ball V Protein Adsorption on Dopamine-Melanin Films: Role of Electrostatic Interactions Inferred from Zeta-Potential Measurements *versus* Chemisorption. J. Colloid Interf. Sci 2010, 344, 54–60.

(44). Li YX ; Li J ; Shangguan E ; Li QM The Effect of Acidity, Hydrogen Bond Catalysis and Auxiliary Electrode Reaction on the Oxidation Peak Current for Dopamine, Uric Acid and Tryptophan. Anal. Methods 2015, 7, 2636–2644.

(45). Zaidi KU ; Ali AS ; Ali SA ; Naaz I Microbial Tyrosinases: Promising Enzymes for Pharmaceutical, Food Bioprocessing, and Environmental Industry. Biochem. Res. Int 2014, 2014, 854687.24895537

(46). Han XF ; Zhang L ; Li CZ Preparation of Polydopamine-Functionalized Graphene-Fe_3O_4 Magnetic Composites with High Adsorption Capacities. RSC Adv 2014, 4, 30536–30541.

(47). Chambrion P ; Suzuki T ; Zhang ZG ; Kyotani T ; Tomita A XPS of Nitrogen-Containing Functional Groups Formed During the C-NO Reaction. Energ. Fuel 1997, 11, 681–685.

(48). Noel S ; Liberelle B ; Robitaille L ; De Crescenzo G Quantification of Primary Amine Groups Available for Subsequent Biofunctionalization of Polymer Surfaces. Bioconjugate Chem 2011, 22, 1690–1699.

(49). Han L ; Lu X ; Liu K ; Wang K ; Fang L ; Weng LT ; Zhang H ; Tang Y ; Ren F ; Zhao C ; Sun G ; Liang R ; Li Z Mussel-Inspired Adhesive and Tough Hydrogel Based on Nanoclay Confined Dopamine Polymerization. ACS Nano 2017, 11, 2561–2574.28245107

(50). Hadjidemetriou M ; Kostarelos K Nanomedicine Evolution of the Nanoparticle Corona. Nat. Nanotechnol 2017, 12, 288–290.28383044

(51). Pelaz B ; del Pino P ; Maffre P ; Hartmann R ; Gallego M ; Rivera-Fernandez S ; de la Fuente JM ; Nienhaus GU ; Parak WJ Surface Functionalization of Nanoparticles with Polyethylene Glycol: Effects on Protein Adsorption and Cellular Uptake. ACS Nano 2015, 9, 6996–7008.26079146

(52). Lai ZW ; Yan Y ; Caruso F ; Nice EC Emerging Techniques in Proteomics for Probing Nano-Bio Interactions. ACS Nano 2012, 6, 10438–10448.23214939

(53). Milani S ; Bombelli FB ; Pitek AS ; Dawson KA ; Radler J Reversible *versus* Irreversible Binding of Transferrin to Polystyrene Nanoparticles: Soft and Hard Corona. ACS Nano 2012, 6, 2532–2541.22356488

(54). Walkey CD ; Chan WCW Understanding and Controlling the Interaction of Nanomaterials with Proteins in a Physiological Environment. Chem. Soc. Rev 2012, 41, 2780–2799.22086677

(55). Horbett TA Principles Underlying the Role of Adsorbed Plasma-Proteins in Blood Interactions with Foreign Materials. Cardiovasc. Pathol 1993, 2, S137–S148.

(56). Lishko VK ; Podolnikova NP ; Yakubenko VP ; Yakovlev S ; Medved L ; Yadav SP ; Ugarova TP Multiple Binding Sites in Fibrinogen for Integrin $A_M\beta_2$ (Mac-1). J. Biol. Chem 2004, 279, 44897–44906.15304494

(57). Lundqvist M ; Stigler J ; Elia G ; Lynch I ; Cedervall T ; Dawson KA Nanoparticle Size and Surface Properties Determine the Protein Corona with Possible Implications for Biological Impacts. Proc. Natl. Acad. Sci. U.S.A 2008, 105, 14265–14270.18809927

(58). Mariam J ; Sivakami S ; Dongre PM Albumin Corona on Nanoparticles − A Strategic Approach in Drug Delivery. Drug Deliv 2016, 23, 2668–2676.26056719

(59). Moghimi SM ; Andersen AJ ; Ahmadvand D ; Wibroe PP ; Andresen TL ; Hunter AC Material Properties in Complement Activation. Adv. Drug Deliv. Rev 2011, 63, 1000–1007.21689701

(60). Cifuentes-Rius A ; de Puig H ; Kah JC ; Borros S ; Hamad-Schifferli K Optimizing the Properties of the Protein Corona Surrounding Nanoparticles for Tuning Payload Release. ACS Nano 2013, 7, 10066–10074.24128271

(61). Mortimer GM ; Butcher NJ ; Musumeci AW ; Deng ZJ ; Martin DJ ; Minchin RF Cryptic Epitopes of Albumin Determine Mononuclear Phagocyte System Clearance of Nanomaterials. ACS Nano 2014, 8, 3357–3366.24617595

(62). Sim RB ; Tsiftsoglou SA Proteases of the Complement System. Biochem. Soc. Trans 2004, 32, 21–27.14748705

(63). Rybak-Smith MJ ; Sim RB Complement Activation by Carbon Nanotubes. Adv. Drug Deliv. Rev 2011, 63, 1031–1041.21669239

(64). Mirshafiee V ; Mahmoudi M ; Lou K ; Cheng J ; Kraft ML Protein Corona Significantly Reduces Active Targeting Yield. Chem. Commun 2013, 49, 2557–2559.

(65). Allen TM ; Hansen C ; Martin F ; Redemann C ; Yau-Young A Liposomes Containing Synthetic Lipid Derivatives of Poly(Ethylene Glycol) Show Prolonged Circulation Half-Lives *in Vivo*. Biochim. Biophys. Acta 1991, 1066, 29–36.2065067

(66). Mahmoudi M ; Lynch I ; Ejtehadi MR ; Monopoli MP ; Bombelli FB ; Laurent S Protein −Nanoparticle Interactions: Opportunities and Challenges. Chem. Rev 2011, 111, 5610–5637.21688848

(67). Schöttler S ; Becker G ; Winzen S ; Steinbach T ; Mohr K ; Landfester K ; Mailänder V ; Wurm FR Protein Adsorption is Required for Stealth Effect of Poly(Ethylene Glycol)- and Poly(Phosphoester)-Coated Nanocarriers. Nat. Nanotechnol 2016, 11, 372–377.26878141

(68). Tenzer S ; Docter D ; Rosfa S ; Wlodarski A ; Kuharev J ; Rekik A ; Knauer SK ; Bantz C ; Nawroth T ; Bier C ; Sirirattanapan J ; Mann W ; Treuel L ; Zellner R ; Maskos M ; Schild H ; Stauber RH Nanoparticle Size is a Critical Physicochemical Determinant of the Human Blood Plasma Corona: A Comprehensive Quantitative Proteomic Analysis. ACS Nano 2011, 5, 7155–7167.21866933

(69). Goppert TM ; Muller RH Adsorption Kinetics of Plasma Proteins on Solid Lipid Nanoparticles for Drug Targeting. Int. J. Pharm 2005, 302, 172–186.16098695

(70). Aoyama M ; Hata K ; Higashisaka K ; Nagano K ; Yoshioka Y ; Tsutsumi Y Clusterin in the Protein Corona Plays a Key Role in the Stealth Effect of Nanoparticles against Phagocytes. Biochem. Biophys. Res. Commun 2016, 480, 690–695.27983983

(71). Lee YK ; Choi EJ ; Webster TJ ; Kim SH ; Khang D Effect of the Protein Corona on Nanoparticles for Modulating Cytotoxicity and Immunotoxicity. Int. J. Nanomedicine 2015, 10, 97–113.25565807

(72). Yan H ; Teh C ; Sreejith S ; Zhu LL ; Kwok A ; Fang WQ ; Ma X ; Nguyen KT ; Korzh V ; Zhao YL Functional Mesoporous Silica Nanoparticles for Photothermal-Controlled Drug Delivery *in Vivo*. Angew. Chem. Int. Edit 2012, 51, 8373–8377.

(73). Song GS ; Liang C ; Gong H ; Li MF ; Zheng XC ; Cheng L ; Yang K ; Jiang XQ ; Liu Z Core-Shell MnSe@Bi_2Se_3 Fabricated *via* a Cation Exchange Method as Novel Nanotheranostics for Multimodal Imaging and Synergistic Thermoradiotherapy. Adv. Mater 2015, 27, 6110–6117.26331476

(74). Kah JC ; Chen J ; Zubieta A ; Hamad-Schifferli K Exploiting the Protein Corona around Gold Nanorods for Loading and Triggered Release. ACS Nano 2012, 6, 6730–6740.22804333

(75). Zou LL ; Wang H ; He B ; Zeng LJ ; Tan T ; Cao HQ ; He XY ; Zhang ZW ; Guo SR ; Li YP Current Approaches of Photothermal Therapy in Treating Cancer Metastasis with Nanotherapeutics. Theranostics 2016, 6, 762–772.27162548

(76). Yang F ; Teves SS ; Kemp CJ ; Henikoff S Doxorubicin, DNA Torsion, and Chromatin Dynamics. Biochim. Biophys. Acta 2014, 1845, 84–89.24361676

(77). Mrowczynski R ; Jurga-Stopa J ; Markiewicz R ; Coy EL ; Jurga S ; Wozniak A Assessment of Polydopamine Coated Magnetic Nanoparticles in Doxorubicin Delivery. RSC Adv 2016, 6, 5936–5943.

(78). Li M ; Gao Y ; Yuan YY ; Wu YZ ; Song ZF ; Tang BZ ; Liu B ; Zheng QC One-Step Formulation of Targeted Aggregation-Induced Emission Dots for Image-Guided Photodynamic Therapy of Cholangiocarcinoma. ACS Nano 2017, 11, 3922–3932.28383899

(79). Li CY ; Liu ZJ ; Yao P Gold Nanoparticles Coated with a Polydopamine Layer and Dextran Brush Surface for Diagnosis and Highly Efficient Photothermal Therapy of Tumors. RSC Adv 2016, 6, 33083–33091.

(80). Vovusha H ; Sanyal S ; Sanyal B Interaction of Nucleobases and Aromatic Amino Acids with Graphene Oxide and Graphene Flakes. J. Phys. Chem. Lett 2013, 4, 3710–3718.

(81). Mudedla S ; Balamurugan K ; Subramanian V Computational Study on the Interaction of Modified Nucleobases with Graphene and Doped Graphenes. J. Phys. Chem. C 2014, 118, 16165–16174.

(82). Bahlakeh G ; Hasani-Sadrabadi MM ; Jacob KI Exploring the Hydrated Microstructure and Molecular Mobility in Blend Polyelectrolyte Membranes by Quantum Mechanics and Molecular Dynamics Simulations. RSC Adv 2016, 6, 35517–35526.

(83). Hasani-Sadrabadi MM ; Taranejoo S ; Dashtimoghadam E ; Bahlakeh G ; Majedi FS ; VanDersarl JJ ; Janmaleki M ; Sharifi F ; Bertsch A ; Hourigan K ; Tayebi L ; Renaud P ; Jacob KI Microfluidic Manipulation of Core/Shell Nanoparticles for Oral Delivery of Chemotherapeutics: A New Treatment Approach for Colorectal Cancer. Adv. Mater 2016, 28, 4134–4141.27001745

(84). Bahlakeh G ; Mahdi Hasani-Sadrabadi M ; Jacob KI Morphological and Transport Characteristics of Swollen Chitosan-Based Proton Exchange Membranes Studied by Molecular Modeling. Biopolymers 2017, 107, 5–19.27588722

(85). Hasani-Sadrabadi MM ; Dashtimoghadam E ; Bahlakeh G ; Majedi FS ; Keshvari H ; Van Dersarl JJ ; Bertsch A ; Panahifar A ; Renaud P ; Tayebi L ; Mahmoudi M ; Jacob KI On-Chip Synthesis of Fine-Tuned Bone-Seeking Hybrid Nanoparticles. Nanomedicine 2015, 10, 3431–3449.26607456

(86). Bahlakeh G ; Ramezanzadeh B A Detailed Molecular Dynamics Simulation and Experimental Investigation on the Interfacial Bonding Mechanism of an Epoxy Adhesive on Carbon Steel Sheets Decorated with a Novel Cerium–Lanthanum Nanofilm. ACS Appl. Mater. Interf 2017, 9, 17536–17551.

(87). Bae JE ; Kim IJ ; Nam KH Disruption of the Hydrogen Bonding Network Determines the pH-Induced Non-Fluorescent State of the Fluorescent Protein Zsyellow by Protonation of Glu221. Biochem. Biophys. Res. Commun 2017, 493, 562–567.28867188

(88). Gronthos S ; Mankani M ; Brahim J ; Robey PG ; Shi S Postnatal Human Dental Pulp Stem Cells (DPSCs) *in Vitro* and *in Vivo*. Proc. Natl. Acad. Sci. U.S.A 2000, 97, 13625–13630.11087820

(89). Seo B-M ; Miura M ; Gronthos S ; Bartold PM ; Batouli S ; Brahim J ; Young M ; Robey PG ; Wang CY ; Shi S Investigation of Multipotent Postnatal Stem Cells from Human Periodontal Ligament. Lancet 2004, 364, 149–155.15246727

(90). Palchetti S ; Colapicchioni V ; Digiacomo L ; Caracciolo G ; Pozzi D ; Capriotti AL ; La Barbera G ; Laganà A The Protein Corona of Circulating PEGylated Liposomes. Biochim. Biophys. Acta 2016, 1858, 189–196.

(91). Zhao Y ; Schultz NE ; Truhlar DG Design of Density Functionals by Combining the Method of Constraint Satisfaction with Parametrization for Thermochemistry, Thermochemical Kinetics, and Noncovalent Interactions. J. Chem. Theory. Comput 2006, 2, 364–382.26626525

(92). McLean AD ; Chandler GS Contracted Gaussian Basis Sets for Molecular Calculations. I. Second Row Atoms, Z=11–18. J. Chem. Phys 1980, 72, 5639–5648.

(93). Lee C ; Yang W ; Parr RG Development of the Colle-Salvetti Correlation-Energy Formula into a Functional of the Electron Density. Phys. Rev. B 1988, 37, 785–789.

(94). Becke AD Density-Functional Thermochemistry. III. The Role of Exact Exchange. J. Chem. Phys 1993, 98, 5648–5652.

(95). Breneman CM ; Wiberg KB Determining Atom-Centered Monopoles from Molecular Electrostatic Potentials. The Need for High Sampling Density in Formamide Conformational Analysis. J. Comput. Chem.c 1990, 11, 361–373.

(96). Frisch M ; Trucks G ; Schlegel HB ; Scuseria G ; Robb M ; Cheeseman J ; Scalmani G ; Barone V ; Mennucci B ; Petersson G ; Gaussian, Inc., Wallingford CT: 2009.

(97). Accelrys Software Inc., S. D, 2009.

(98). Sun H Compass: An *Ab Initio* Force-Field Optimized for Condensed-Phase Applications Overview with Details on Alkane and Benzene Compounds. J. Phys. Chem. B 1998, 102, 7338–7364.

(99). Sun H ; Ren P ; Fried J The Compass Force Field: Parameterization and Validation for Phosphazenes. Comput. Theor. Polym. Sci 1998, 8, 229–246.

(100). Chai D ; Xie Z ; Wang Y ; Liu L ; Yum Y-J Molecular Dynamics Investigation of the Adhesion Mechanism Acting between Dopamine and the Surface of Dopamine-Processed Aramid Fibers. ACS Appl. Mater. Interf 2014, 6, 17974–17984.

(101). Swope WC ; Andersen HC ; Berens PH ; Wilson KR A Computer Simulation Method for the Calculation of Equilibrium Constants for the Formation of Physical Clusters of Molecules: Application to Small Water Clusters. J. Chem. Phys 1982, 76, 637–649.

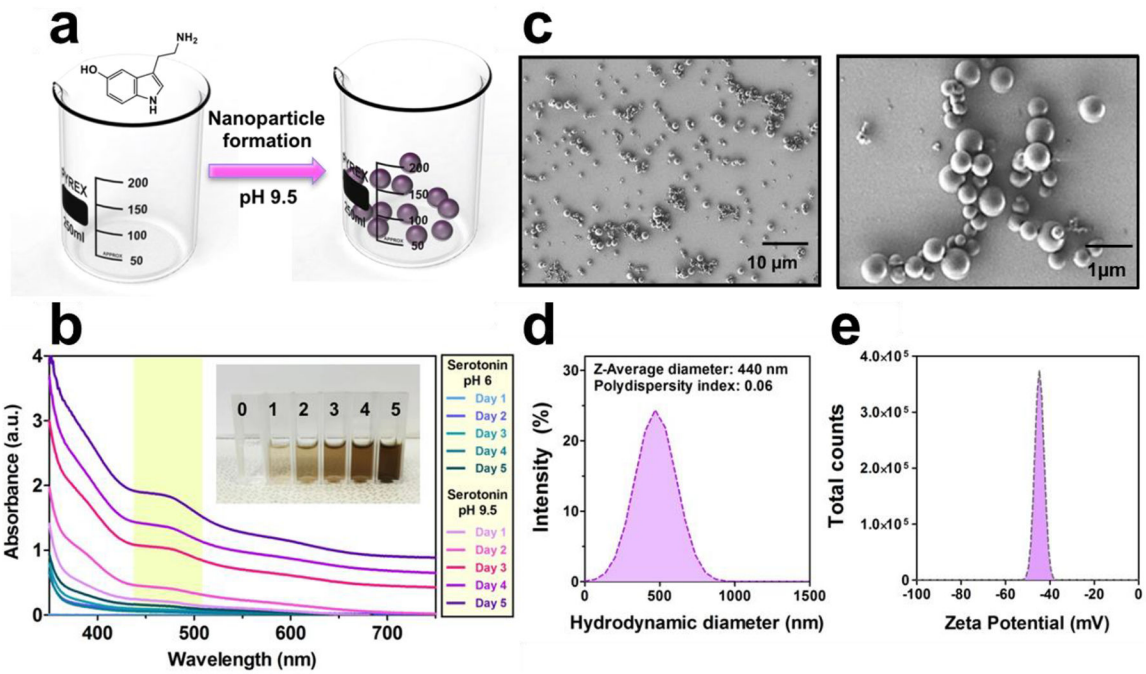

Figure 1.

(a) Schematic illustration of the synthesis of polyserotonin nanoparticles (not to scale). (b) UV-vis absorption spectra for aqueous solutions of serotonin incubated at either pH 6 or pH 9.5 over 5 days with a photograph of cuvettes containing samples at each time point under basic conditions. (c) Scanning electron microscope images of polyserotonin nanoparticles after 5 days. (d) Average sizes of polyserotonin nanoparticles determined to be 440 nm *via* dynamic light scattering with a polydispersity index of 0.06 after 5 days. (e) Zeta potential of polyserotonin nanoparticles.

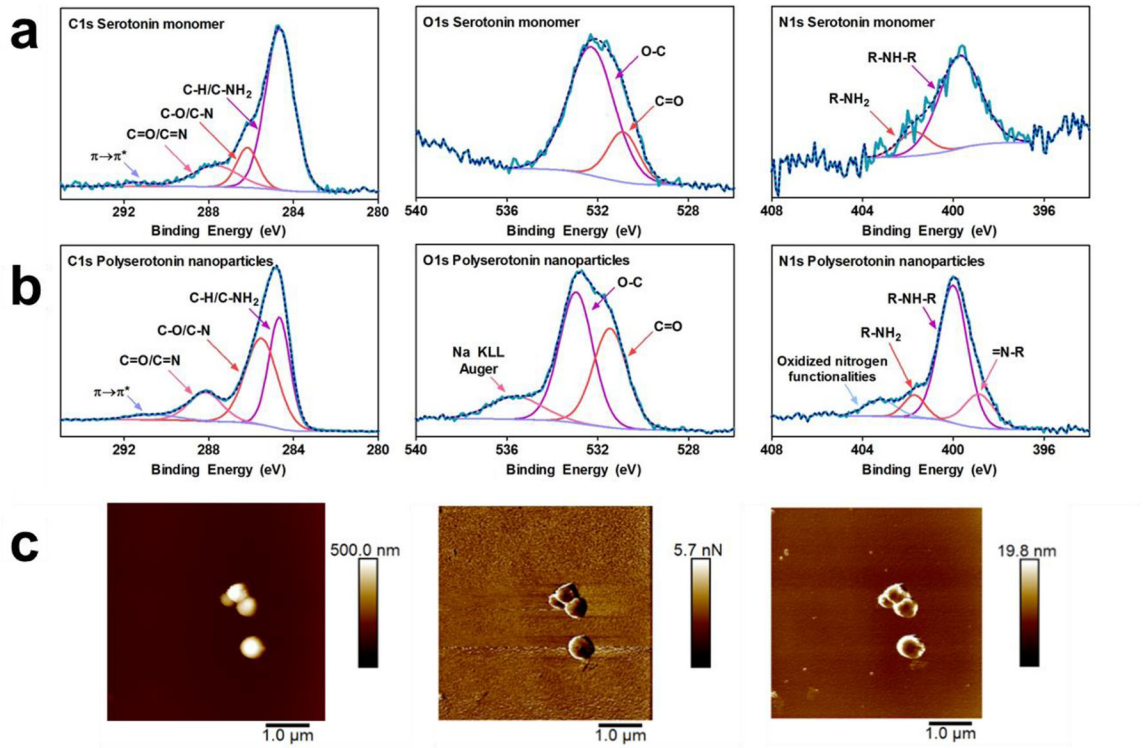

Figure 2.

Characterization of polyserotonin nanoparticles. (a) XPS spectra for the C 1s, O 1s, and N 1s peaks for serotonin incubated at acidic pH to prevent nanoparticle formation. (b) XPS spectra for the C 1s, O 1s, and N 1s peaks for serotonin incubated at basic pH to induce polymerization and nanoparticle formation. Fitted curves are labeled with the corresponding species. The dashed lines in the spectra represent the global envelopes corresponding to the sum of the Gaussian-Lorentzian peaks used to fit the spectra. (c) Atomic force microscopy images of serotonin nanoparticles showing height, adhesion, and deformation.

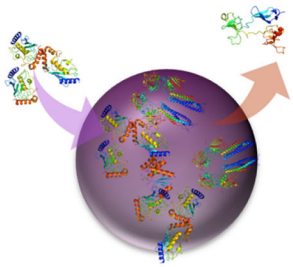

Protein class	Protein	PDA	PST	PDA-PEG	PST-PEG	%
Acute Phase	Fibronectin	0.55	0.56	3.54	2.39	100.00
	Other	0.42	0.44	3.50	2.78	90.00
Coagulation Protein	Fibrinogen	40.13	38.76	5.17	5.72	80.00
	Other	0.58	0.63	0.25	0.04	70.00
Complement Proteins		1.63	1.67	5.28	6.26	60.00
Immunoglobulins		7.62	7.86	7.03	6.63	50.00
Lipoproteins	Apolipoprotein	2.42	3.37	15.29	18.94	40.00
	Clusterin	3.56	4.52	40.12	47.09	30.00
	Other	0.88	0.91	0.28	0.34	20.00
Plasma Component	Serum Albumin	29.87	28.78	9.95	4.29	10.00
	Other	0.75	0.65	0.70	0.42	5.00
Tissue Leakage	Vitronectin	10.92	11.07	5.48	4.18	2.00
	Other	0.68	0.79	3.41	0.93	0.00
	SUM (%)	100	100	100	100	
	Total Protein Content (fmol)	973.17	625.60	233.80	219.15	
	Ratio	1.00	0.64	0.24	0.23	

Figure 3.

Protein corona measurements. (a) Schematic of presumptive interactions with plasma proteins and polyserotonin nanoparticles. (b) Heat map of the adsorbed proteins on polydopamine (PDA), polyserotonin (PST), PEGylated PDA, and PEGylated PST nanoparticles, evaluated by proteomic mass spectrometry and ordered based on abundances. Averages from triplicate measurements are reported in femtomoles. Percentages of identified proteins are grouped according to biological class.

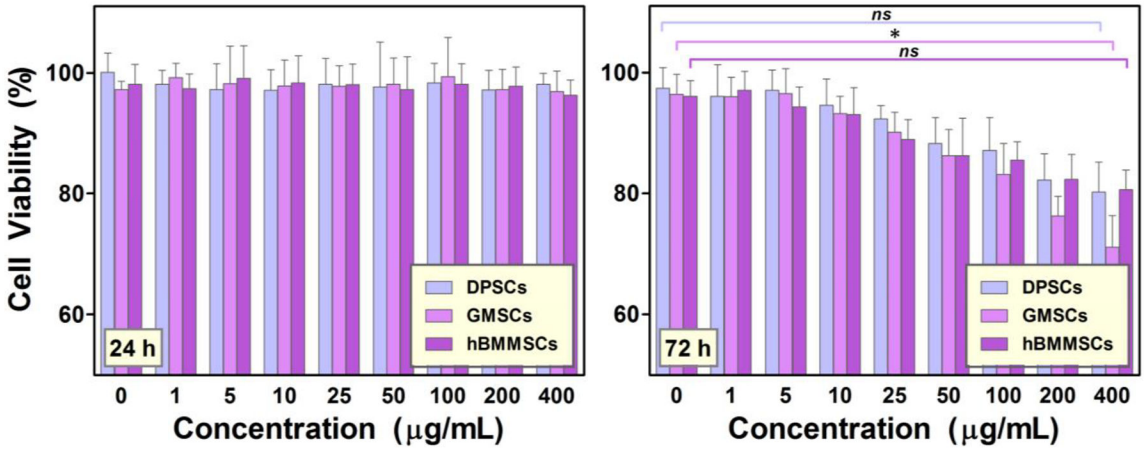

Figure 4.

Viability of human dental pulp stem cells (DPSCs), gingival-derived mesenchymal stem cells (GMSCs), and human bone-marrow mesenchymal stem cells, (hBMMSCs) after incubation with different concentrations of polyserotonin nanoparticles for 24 h (left) or 72 h (right). Comparing the viability of stem cells alone with cells incubated with the highest concentration of polyserotonin nanoparticles (400 μg/mL) for 72 h, mean viability was statistically lower only for GMSCs [$t(4)=4.074$; $P<0.05$]. Changes in viability for the DPSCs and hBMMSCs were not statistically significant.

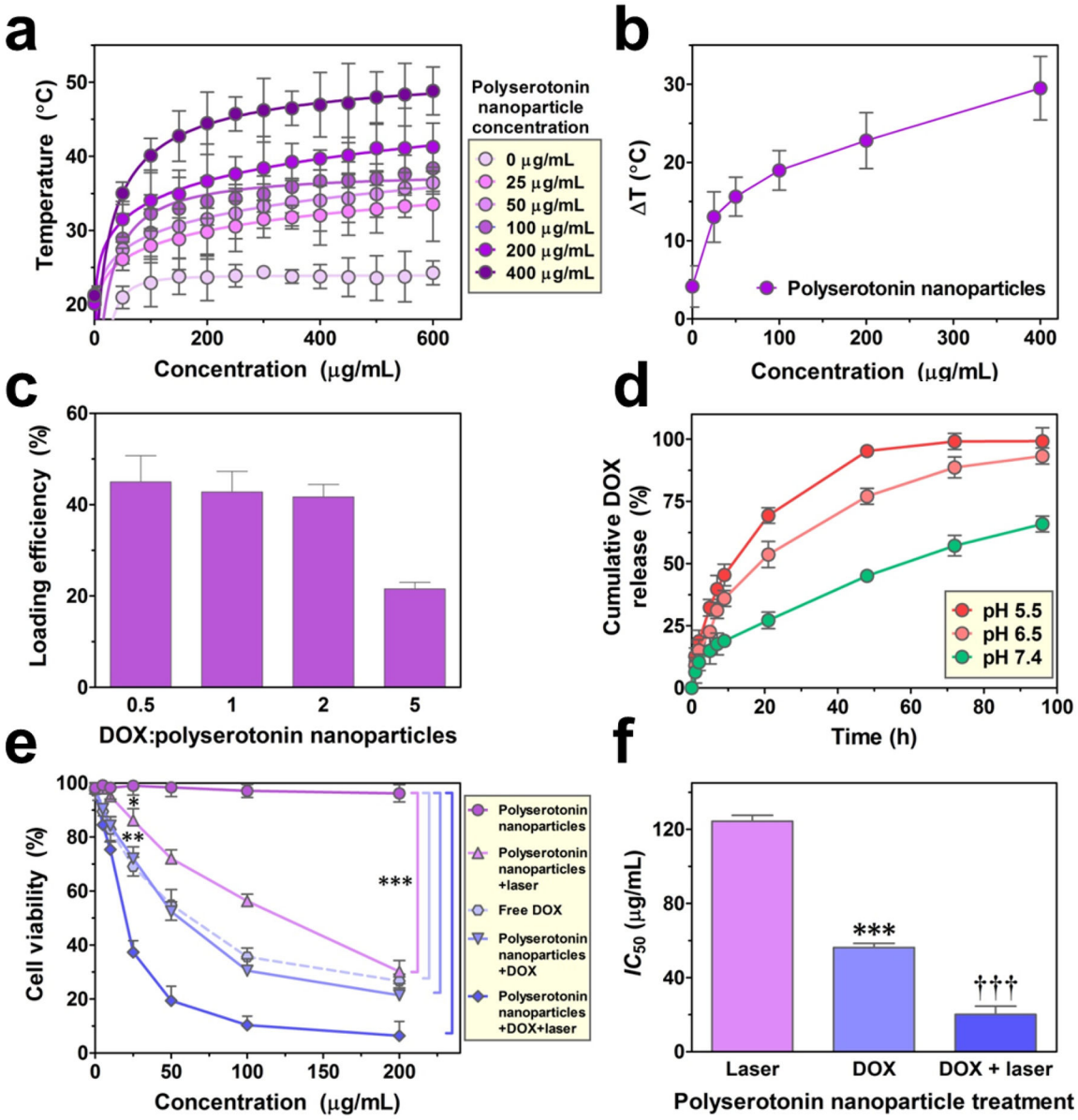

Figure 5.

(a) *In vitro* heat generation in Dulbecco's Modified Eagle medium (DMEM) suspensions containing various concentrations of polyserotonin nanoparticles after NIR-irradiation (808 nm laser; 3 W·cm^{-2}; 10 min). (b) Temperature changes (ΔT) after 10 min for various concentrations of polyserotonin nanoparticles after NIR-irradiation. (c) Loading efficiencies of doxorubicin (DOX) on the surfaces of polyserotonin nanoparticles at different drug/nanoparticle ratios relative to 1 mg/mL nanoparticle concentrations. (d) Cumulative *in vitro* release profiles of DOX from polyserotonin-based nanoparticles in PBS at different pH values mimicking tumor microenvironments (pH 6.5) and intracellular endosomal environments (pH 5.5). (e) 3-(4,5-Dimethylthiazol-2-yl)-2,5-diphenyltetrazolium bromide (MTT) cell viability assay of HeLa cells after 24 h exposures to DOX-loaded (2:1 ratio) *vs.* unloaded polyserotonin nanoparticles as a function of particle concentration at 37 °C. HeLa

cell viability for free DOX is shown for reference (dashed line). The combined effects of laser exposure and DOX treatment (DOX-loaded nanoparticles + laser exposure) on the viability of HeLa cells are also shown. (f) Estimated half maximal inhibitory concentrations (IC_{50}) for polyserotonin-based nanotherapeutics. Error bars are standard errors of the means (N=3). Group means were significantly different [$F(2,6)=719$; $P<0.001$]; ***$P<0.001$ *vs.* laser or DOX+laser treatment; $^{\dagger\dagger\dagger}P<0.001$ *vs.* laser or DOX treatment.

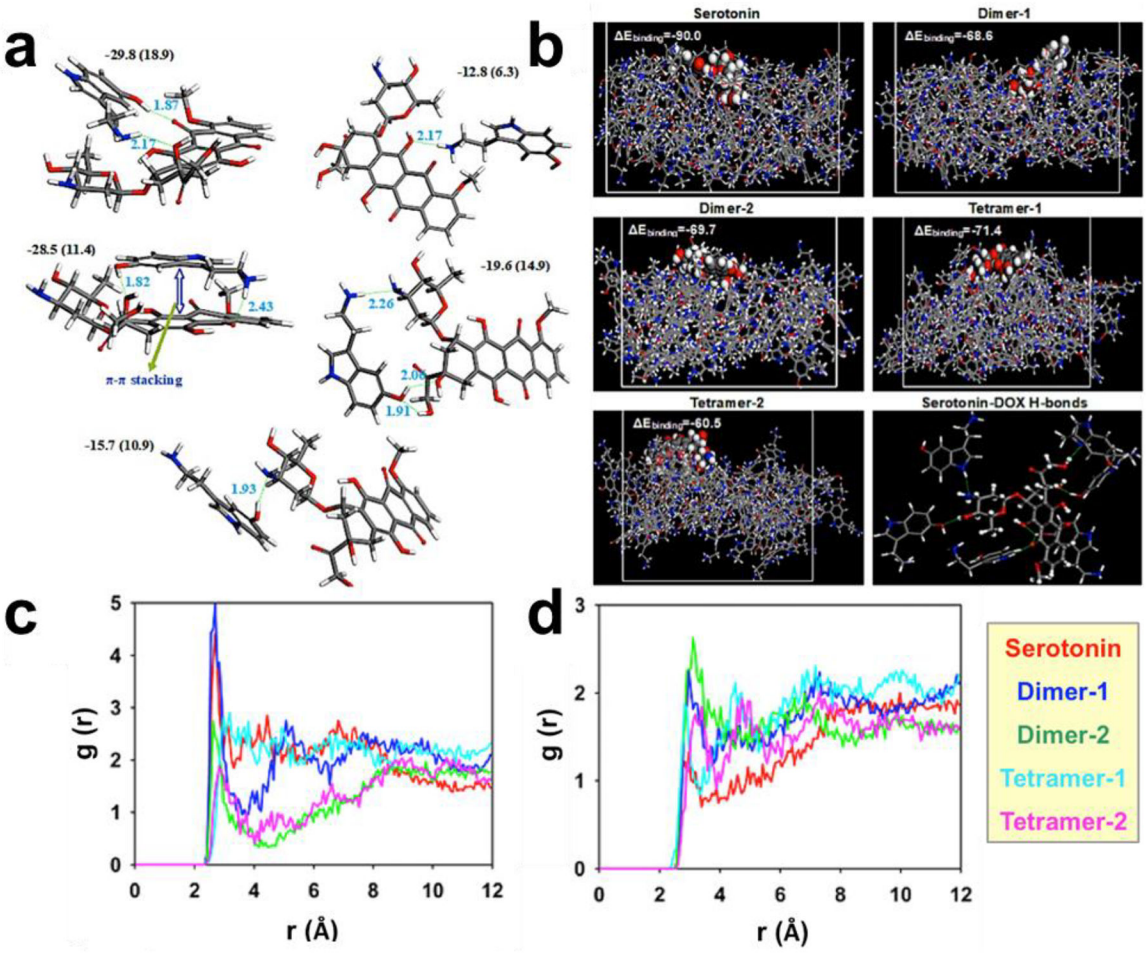

Figure 6.

Investigation of molecular interactions between serotonin-based clusters and the drug molecule, doxorubicin (DOX). (a) The DFT M06–2X/6–311G(d,p) optimized geometries of different DOX-serotonin clusters. The hydrogen bonds are shown as green dashed lines and their lengths are in Ångstroms. The computed binding energies are in kcal/mol. The data in parentheses indicate the binding energies derived from the DFT/B3LYP/6–311G(d,p) theory level. (b) Side views of final snapshots of a DOX molecule on the surface of monomeric serotonin or two dimers or tetramers were obtained from molecular dynamics simulations. The DOX molecule is displayed in CPK style. The hydrogen-bonding interactions of surface-bound DOX with serotonin molecules are shown as green dashed lines. Radial distribution functions of oxygen atoms in DOX with (c) oxygen and (d) nitrogen atoms in monomeric, dimeric, or tetrameric serotonin.

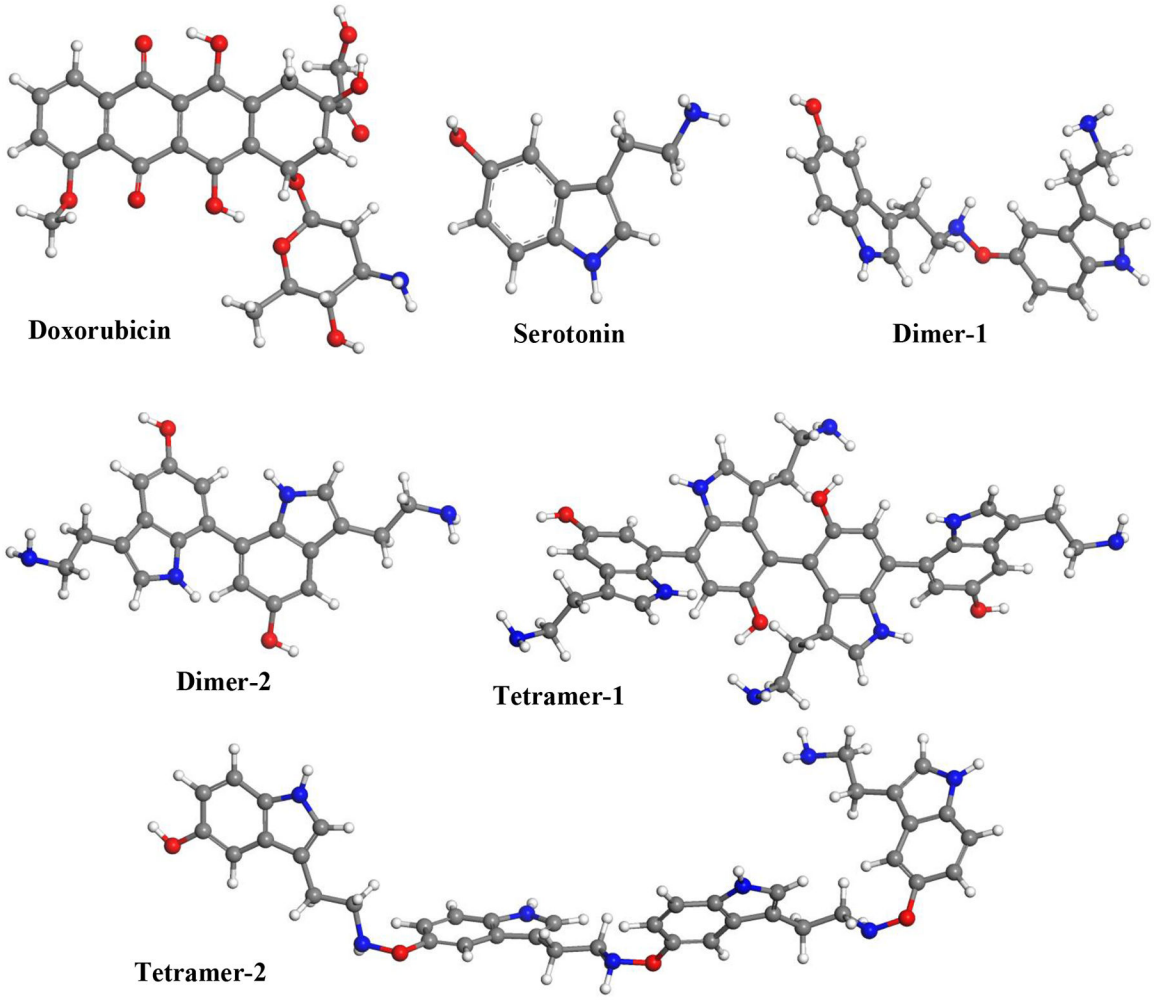

Scheme 1.

The B3LYP/6–311G(d,p) optimized geometries of doxorubicin (DOX), serotonin, and the constructed serotonin dimers and tetramers selected for theoretical QM calculations and MD simulations. The atomic color code is: carbon gray, oxygen red, hydrogen white, and nitrogen blue.